Effect of resonance decay on conserved number fluctuations in a hadron resonance gas model

D. K. Mishra,[1,*] P. Garg,[2] P. K. Netrakanti,[1] and A. K. Mohanty[1,†]
[1]*Nuclear Physics Division, Bhabha Atomic Research Center, Mumbai 400085, India*
[2]*Department of Physics and Astronomy, Stony Brook University, SUNY, Stony Brook, New York 11794-3800, USA*
(Received 27 April 2016; published 18 July 2016)

We study the effect of charged secondaries coming from resonance decay on the net-baryon, net-charge, and net-strangeness fluctuations in high-energy heavy-ion collisions within the hadron resonance gas (HRG) model. We emphasize the importance of including weak decays along with other resonance decays in the HRG, while comparing with the experimental observables. The effect of kinematic cuts on resonances and primordial particles on the conserved number fluctuations are also studied. The HRG model calculations with the inclusion of resonance decays and kinematical cuts are compared with the recent experimental data from STAR and PHENIX experiments. We find good agreement between our model calculations and the experimental measurements for both net-proton and net-charge distributions.

DOI: 10.1103/PhysRevC.94.014905

I. INTRODUCTION

The Beam Energy Scan (BES) program at Brookhaven National Laboratory's Relativistic Heavy-Ion Collider (RHIC) has drawn much attention to explore the quantum chromodynamics (QCD) phase diagram in terms of temperature T and baryon chemical potential μ_B [1–4]. Several theoretical models suggest the existence of a critical point in the T-μ_B plane where the first-order phase-transition line originating from high μ_B ends [5–7]. The location of the critical point can be explored by systematically varying T and μ_B. Experimentally, one can vary T and μ_B by varying the center-of-mass energy of the colliding ions. It has been suggested that the excitation function of conserved numbers such as net-baryon, net-charge, and net-strangeness fluctuations should show a nonmonotonic behavior as a possible signature of QCD critical end point (CEP) [8–10].

In the thermodynamic limit, the correlation length ξ diverges at the CEP [1]. The moments of the net-baryon, net-charge, and net-strangeness distributions are related to the ξ of the system and hence these moments can be used to look for signals of a phase transition and critical point [11,12]. Also, the comparison of experimentally measured cumulants with the lattice calculations enables us to extract the freeze-out parameters i.e., freeze-out temperature T_f and μ_B, of the system produced in heavy-ion collisions [13–15]. In recent years, lots of effort has been applied on both theoretical and experimental fronts to study the fluctuation of conserved quantities. Current experiments at RHIC (PHENIX and STAR) have reported their measurements of higher moments for net-charge [15,16] and for net-proton [17] multiplicity distributions at different center-of-mass energies ($\sqrt{s_{NN}}$) using the data from the BES. Experimentally, the net-baryon number fluctuations are not directly measured, because not all neutral baryons are detected by most of the experiments. Hence, net-baryon fluctuations are accessible via measuring the net-proton distributions [18]. The net-charge fluctuations are accessible by measuring the stable charged particles such as pions, kaons, and protons along with their antiparticles [15,16]. Similarly, the measurement of net-kaon fluctuations act as proxy for net-strangeness fluctuations, because higher mass strange particles are not directly measured. There are several sources of nonequilibrium fluctuations that can diminish the fluctuations measured by experiments [19]. It is important to identify the noncritical baseline to understand the critical properties of different conserved number fluctuations.

Experimentally measured moments of the net distributions are related to the cumulants as follows: mean $M = C_1$; variance $\sigma^2 = C_2 = \langle(\delta N)^2\rangle$; skewness $S = C_3/C_2^{3/2} = \langle(\delta N)^3\rangle/\sigma^3$, and kurtosis $\kappa = C_4/C_2^2 = \langle(\delta N)^4\rangle/\sigma^4 - 3$, where N is the multiplicity of the distribution and $\delta N = N - M$. Hence, the ratios of the cumulants are related to the moments as follows: $\sigma^2/M = C_2/C_1$, $S\sigma = C_3/C_2$, $\kappa\sigma^2 = C_4/C_2$, and $S\sigma^3/M = C_3/C_1$. Furthermore, the ratios moments/cumulants can be related to the susceptibilities of nth order (χ^n) obtained from the lattice QCD or the HRG model calculations as $\sigma^2/M \sim \chi^{(2)}/\chi^{(1)}$, $S\sigma \sim \chi^{(3)}/\chi^{(2)}$, $\kappa\sigma^2 \sim \chi^{(4)}/\chi^{(2)}$, and $S\sigma^3/M \sim \chi^{(3)}/\chi^{(1)}$. One advantage of measuring the ratios is that the dependence of volume on the experimental measured individual cumulants cancel out in the ratios. Experimentally, one measures only the final abundance of hadrons, which includes both primordial particle production as well as contributions from the resonance decays. Production of resonances play an important role for studying various properties of interaction dynamics in the heavy-ion collisions. Resonances having short lifetime that subsequently decay into stable hadrons and can affect the final hadron yields and their number fluctuations.

The HRG model has been successful in explaining the particles produced in heavy-ion collisions from energies typical of the Brookhaven National Laboratory Alternating Gradient Synchrotron (AGS) to those of the Large Hadron Collider (LHC) [20–22]. The susceptibilities and their ratios in hadronic phase calculated in the HRG model reasonably agree with the lattice QCD results at lower μ_B [12]. Several studies

*dkmishra@rcf.rhic.bnl.gov
†Presently at Saha Institute of Nuclear Physics, 1/AF, Bidhan Nagar, Kolkata 700064, India.

have been performed with the HRG model for the fluctuation of conserved quantities, which are considered as baselines for such measurements [23–27]. Also, similar baseline studies have been performed by using independent production models and transport models [28–31] . Keeping in mind the existence of CEP in the QCD phase diagram and the efforts applied on both the theoretical and experimental sides, it is important to calculate the more appropriate baseline for comparison with experimental data. In the present work, we estimate the contribution of resonances to the conserved number fluctuation by using the HRG model. As discussed in Ref. [32], we also calculate the effect of average decay and by considering the higher-order correlated terms, the inclusion of weak decays in the model, and the effect of different kinematic cuts on the resonance as well as on the primordial particles. It is important to consider the weak decays because many of the particles which are considered as stable in Ref. [32] decay before reaching the detector. For example, experimentally, η^0 or Λ^0 particles are detected by reconstruction from their decayed daughters which are measured by the detector. Hence their contributions to the fluctuation of stable particles are influenced.

The paper is organized as follows: In the following section, we discuss the HRG model used in this study as well as the implementation of resonance decays. In Sec. III, the results for the observables $\chi^{(2)}/\chi^{(1)}$, $\chi^{(3)}/\chi^{(2)}$, $\chi^{(4)}/\chi^{(2)}$, and $\chi^{(3)}/\chi^{(1)}$ for considering different decay cases as well as inclusion of weak decays and effect of kinematical cuts are discussed. Section IV discuss the comparison of our model calculations to the experimental measurements. Finally, in Sec. V, we summarize our findings and discuss the implication of this work.

II. HADRON RESONANCE GAS MODEL AND RESONANCE DECAYS

The partition function in the HRG model includes all relevant degrees of freedom of the confined, strongly interacting matter and contains all the interactions that result in resonance formation [24]. The heavy-ion experiments cover only a limited phase space, so one can access only a part of the fireball produced in the collision which resembles the grand canonical ensemble [33]. Assuming a thermal system produced in the heavy-ion collisions, the thermodynamic pressure P can be written as sum of the partial pressures of all the particle species i which may be baryon (B) or meson (M):

$$\frac{P}{T^4} = \frac{1}{VT^3}\sum_B \ln Z_i(T,V,\mu_i) + \frac{1}{VT^3}\sum_M \ln Z_i(T,V,\mu_i), \tag{1}$$

where

$$\ln Z_i(T,V,\mu_i) = \pm\frac{Vg_i}{2\pi^2}\int d^3p \ln\{1 \pm \exp[(\mu_i - E)/T]\}, \tag{2}$$

where T is the temperature, V is the volume of the system, μ_i is the chemical potential, and g_i is the degeneracy factor of the ith particle. The total chemical potential of the individual particle is $\mu_i = B_i\mu_B + Q_i\mu_Q + S_i\mu_S$, where B_i, Q_i, and S_i are the baryon, electric charge, and strangeness number of the ith particle, with corresponding chemical potentials μ_B, μ_Q, and μ_S, respectively. The $+ve$ and $-ve$ signs correspond to baryons and mesons, respectively. In a static fireball, a particle of mass m, the volume element (d^3p) can be written as $d^3p = p_T m_T \cosh\eta dp_T d\eta d\phi$ and energy $(E = m_T\cosh\eta)$ of the particle, where m_T is the transverse mass $(m^2 + p_T^2)^{1/2}$, where p_T, η, and ϕ represent the transverse momentum, pseudorapidity, and azimuthal angle, respectively. The experimental acceptances can be applied by considering the corresponding ranges in p_T, η, and ϕ. The fluctuations of the conserved numbers are obtained from the derivative of the thermodynamic pressure with respect to the corresponding chemical potentials μ_B, μ_Q, or μ_S. The nth-order generalized susceptibilities χ are written as

$$\chi_x^{(n)} = \frac{d^n[P(T,\mu)/T^4]}{d(\mu_x/T)^n}. \tag{3}$$

For mesons χ_x can be expressed as

$$\chi_{x,\text{meson}}^{(n)} = \frac{X^n}{VT^3}\int d^3p \sum_{k=0}^{\infty}(k+1)^{n-1} \times\exp\left\{\frac{-(k+1)E}{T}\right\}\exp\left\{\frac{(k+1)\mu}{T}\right\}, \tag{4}$$

and for baryons,

$$\chi_{x,\text{baryon}}^{(n)} = \frac{X^n}{VT^3}\int d^3p \sum_{k=0}^{\infty}(-1)^k(k+1)^{n-1} \times\exp\left\{\frac{-(k+1)E}{T}\right\}\exp\left\{\frac{(k+1)\mu}{T}\right\}, \tag{5}$$

where X represents either B_i, Q_i, or S_i of the ith particle depending on whether the susceptibility χ_x represents net baryon, net electric charge, or net strangeness. The total generalized susceptibilities will be the sum of susceptibility of mesons and baryons as $\chi_x^{(n)} = \sum\chi_{x,\text{mesons}}^{(n)} + \sum\chi_{x,\text{baryons}}^{(n)}$.

In the HRG model, at the chemical freeze-out time, all the particles (primordial as well as resonances) are in equilibrium. The collision energy dependence of freeze-out parameters (μ_B and T_f) are parametrized as given in Ref. [21]. The energy dependence of μ_B is given as, $\mu_B(\sqrt{s_{NN}}) = 1.308/(1 + 0.273\sqrt{s_{NN}})$ and the μ_B dependence of freeze-out temperature is given as $T_f(\mu_B) = 0.166 - 0.139\mu_B^2 - 0.053\mu_B^4$. Furthermore, the ratio of baryon to strangeness chemical potential on the freeze-out curve is parametrized as $\frac{\mu_S}{\mu_B} \simeq 0.164 + 0.018\sqrt{s_{NN}}$. Similarly, the energy dependence of μ_Q and μ_S are parametrized as given in Ref. [24]. In the HRG model, after the production of all the particles, the resonances are allowed to decay to their corresponding daughter particles, thus contributing to the final abundance of the stable meson and baryon numbers. These decay daughters from the resonance can influence the fluctuation of the final hadrons. The ensemble-averaged stable particle yield will have contributions from both primordial production and the resonance decay [23,34],

$$\langle N_i\rangle = \langle N_i^*\rangle + \sum_R \langle N_R\rangle\langle n_i\rangle_R, \tag{6}$$

where $\langle N_i^* \rangle$ and $\langle N_R \rangle$ correspond to the average primordial yield of particle species i and of the resonances R, respectively. The summation runs over all the resonances which decay to the final particle i and $\langle n_i \rangle_R = \sum_r b_r^R n_{i,r}^R$ is the average number of particle type i produced from the resonance R. Furthermore, b_r^R is the branching ratio of the rth decay channel of the resonance R and $n_{i,r}^R$ is the number of particle i produced in that decay branch. The generalized susceptibility for stable particle i of nth order can be written as

$$\chi_i^{(n)} = \chi_i^{*(n)} + \sum_R \chi_R^{(n)} \langle n_i \rangle_R^n. \tag{7}$$

The second term in Eq. (7) includes contributions from fluctuations of primordial resonances and average number of produced particle of type i. We follow Eqs. (17)–(20) from Ref. [32] to calculate the average contributions from the resonances, where we consider fluctuation in the resonance production only and the number of decay daughters are assumed to be fixed. In this work, we refer to this as average decay contributions. For completeness we rewrite the same cumulant equations here as given in Ref. [32]:

$$\langle (\Delta N_i)^2 \rangle = \langle (\Delta N_i^*)^2 \rangle + \sum_R \langle (\Delta N_R)^2 \rangle \langle n_i \rangle_R^2, \tag{8}$$

$$\langle (\Delta N_i)^3 \rangle = \langle (\Delta N_i^*)^3 \rangle + \sum_R \langle (\Delta N_R)^3 \rangle \langle n_i \rangle_R^3, \tag{9}$$

$$\langle (\Delta N_i)^4 \rangle = \langle (\Delta N_i^*)^4 \rangle + \sum_R \langle (\Delta N_R)^4 \rangle \langle n_i \rangle_R^4. \tag{10}$$

Resonance decay processes are probabilistic in nature, which itself causes the final particle number fluctuations. In Eqs. (8)–(10) above, we use $\langle n_i \rangle$, which is same as the sum of the branching ratios of the different decay branches of the resonance. But the number of decay products follow a random distribution which gives fluctuation in the final number of particles. A detailed discussion of resonance decay is given in Refs. [23,26,32]. After considering the fluctuation in the produced daughters, the modified cumulants in Eqs. (8)–(10) of the stable particle from the resonance contributions (full decay) can be written as [32]

$$\langle (\Delta N_i)^2 \rangle = \langle (\Delta N_i^*)^2 \rangle + \sum_R \langle (\Delta N_R)^2 \rangle \langle n_i \rangle_R^2 + \sum_R \langle N_R \rangle \langle (\Delta n_i)^2 \rangle_R, \tag{11}$$

$$\langle (\Delta N_i)^3 \rangle = \langle (\Delta N_i^*)^3 \rangle + \sum_R \langle (\Delta N_R)^3 \rangle \langle n_i \rangle_R^3 + 3 \sum_R \langle (\Delta N_R)^2 \rangle \langle n_i \rangle_R \langle (\Delta n_i)^2 \rangle_R + \sum_R \langle N_R \rangle \langle (\Delta n_i)^3 \rangle_R, \tag{12}$$

$$\langle (\Delta N_i)^4 \rangle = \langle (\Delta N_i^*)^4 \rangle + \sum_R \langle (\Delta N_R)^4 \rangle \langle n_i \rangle_R^4 + 6 \sum_R \langle (\Delta N_R)^3 \rangle \langle n_i \rangle_R^2 \langle (\Delta n_i)^2 \rangle_R + \sum_R \langle (\Delta N_R)^2 \rangle \left[3 \langle (\Delta n_i)^2 \rangle_R^2 + 4 \langle n_i \rangle_R \langle (\Delta n_i)^3 \rangle_R \right] + \sum_R \langle N_R \rangle \langle (\Delta n_i)^4 \rangle_R. \tag{13}$$

Above Eqs. (11)–(13), which we refer to as full decay, the fluctuation of the daughter particles is also considered along with the fluctuation of the resonances. If there is no correlation between the daughter particles, the fluctuation in the multiplicity calculated by using Eqs. (11)–(13) will be very close to the average fluctuation contribution (6)–(10) from resonance decay [32]. The higher-order terms $\langle (\Delta n_i)^2 \rangle_R$, $\langle (\Delta n_i)^3 \rangle_R$, and $\langle (\Delta n_i)^4 \rangle_R$ will be zero for the resonances having only one decay channel or the number of species i being same in each decay branch. Hence, the higher-order terms will have higher contribution for the net-charge and net-kaon cases compared with the net-proton case. In this calculation, we included mesons and baryons of mass up to 2.5 GeV as listed in the particle data book. We consider two different cases: one with weakly decaying particles regarded as stable and in another letting the weakly decaying particles decay into stable ones. In line with Ref. [32], for the first case, we considered 26 weakly decaying particles as stable. By including weak decays in addition to the strongly decaying particles in our analysis, we observe substantial change on the values of cumulant ratios for all the conserved numbers, which we discuss in the following section.

III. RESULTS AND DISCUSSION

Figures 1–3 show the variation of the susceptibility ratios for net-bayon, net-charge, and net-strangeness as a function of the collision energies by considering average-decay [Eqs. (6)–(10)] and full-decay contributions [Eqs. (11)–(13)]

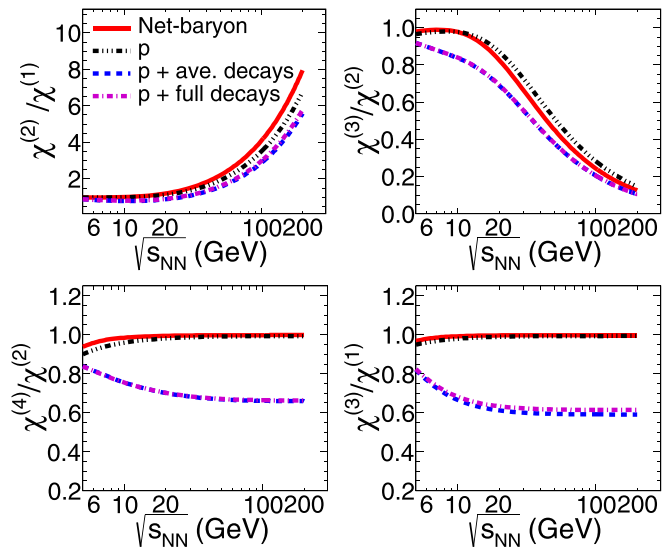

FIG. 1. Collision energy dependence of susceptibility ratios ($\chi^{(2)}/\chi^{(1)}$, $\chi^{(3)}/\chi^{(2)}$, $\chi^{(4)}/\chi^{(2)}$, and $\chi^{(3)}/\chi^{(1)}$) calculated in full phase space for net baryons without resonance decay, primordial protons, and primordial protons with resonance decay including weak-decay resonances.

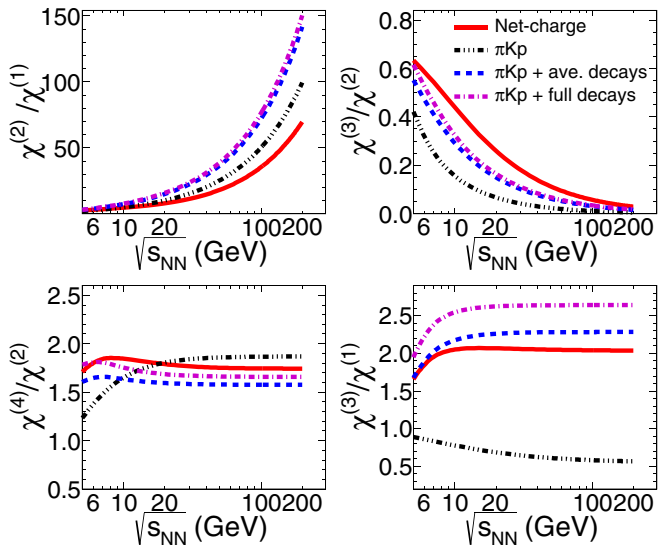

FIG. 2. Collision energy dependence of susceptibility ratios ($\chi^{(2)}/\chi^{(1)}$, $\chi^{(3)}/\chi^{(2)}$, $\chi^{(4)}/\chi^{(2)}$, and $\chi^{(3)}/\chi^{(1)}$) calculated in full phase space for net charge without resonance decay, primordial charged particles (π, K, p), and primordial charged hadrons with resonance decay including weak-decay resonances.

of resonances as discussed in previous section. Figure 1 shows ratios considering all the baryons including the resonances without decay, only primordial protons, primordial protons with average decay contributions from baryonic resonances using Eqs. (6)–(10), and primordial protons with contributions from fluctuation of resonances and their daughter particles (full decay) using Eqs. (11)–(13). Experimentally, net-baryon fluctuations are accessible through net-proton fluctuations.

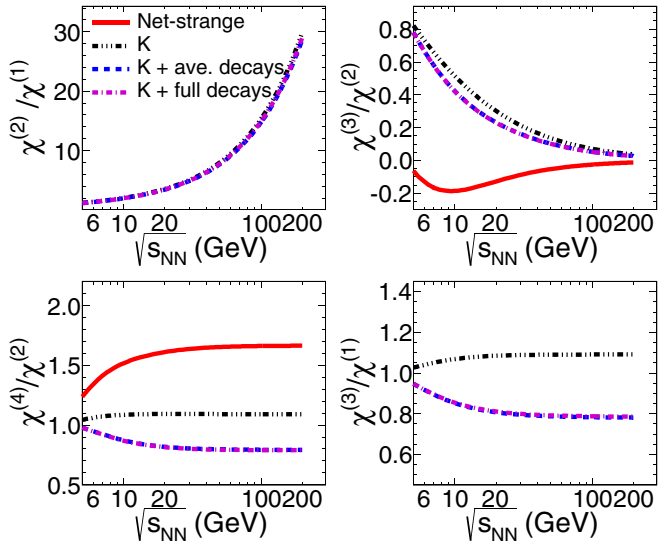

FIG. 3. Collision energy dependence of susceptibility ratios ($\chi^{(2)}/\chi^{(1)}$, $\chi^{(3)}/\chi^{(2)}$, $\chi^{(4)}/\chi^{(2)}$ and $\chi^{(3)}/\chi^{(1)}$) calculated in full phase space for net strangeness without resonance decay, primordial kaons, and primordial kaons with resonance decay including weak-decay resonances.

There is significant effect of decay contributions observed compared with no decay of resonances. However, the difference between average decay and full decay is negligible, which is in agreement with the findings of Ref. [32].

The net-charge fluctuations are accessible through measuring fluctuations of stable charged particles (π, K, and p). Figure 2 shows susceptibility ratios for net charge, which includes all the resonances without decay, only primordial stable charged particles (π, K, and p), primordial particles with average decay contributions from the resonances using Eqs. (6)–(10), and primordial stable particles with full decay contributions using Eqs. (11)–(13). There is substantial change in the susceptibility ratios by including the resonance decay contributions, particularly for higher $\sqrt{s_{NN}}$ of $\chi^{(2)}/\chi^{(1)}$ and $\chi^{(3)}/\chi^{(2)}$ ratios for lower collision energies. The resonance decay effect for net charge is larger compared with net baryon because, in case of baryons, all the baryonic resonances decay into only one baryon in each decay branch, which is not the case for net charge. Most of the higher-mass resonances decay into more than one charged particle. Also the higher-mass resonances again decay into resonance which, after few decay iterations, decay into final stable hadrons. Furthermore, the neutral resonances also contribute to the net-charge fluctuation. For example, consider the ρ^0 meson, which decays into $\pi^+\pi^-$ at about 100%: if both daughter particles are accepted in the detector then the contribution to the mean of the net charge from ρ^0 is zero. In an ideal HRG model in the grand canonical ensemble, thermally produced and noninteracting particles and antiparticles are uncorrelated, so the susceptibility of the net-conserved quantity is $\chi^{(n)}_{\rm net} = \chi^{(n)}_{+} + (-1)^n \chi^{(n)}_{-}$. The second- and fourth-order susceptibilities of ρ^0 will contribute to the net-charge susceptibility because the susceptibility of particle (π^+) and antiparticle (π^-) will be added. But the contribution of ρ^0 to the first- and third-order susceptibilities of the net-charge will be zero. This may be one reason why there is more effect of resonance decay in the $\chi^{(2)}/\chi^{(1)}$ and $\chi^{(3)}/\chi^{(2)}$ ratios.

Experimentally, the net-strangeness fluctuations are accessible through measuring the net-kaon fluctuations. Figure 3 shows the susceptibility ratios of net-strange particles without resonance decay, considering only primordial kaons, primordial kaons with average decay contributions from the strange resonances using Eqs. (6)–(10), and primordial kaons with full decay contributions using Eqs. (11)–(13). For net strangeness there is also significant resonance contributions observed in the $\chi^{(3)}/\chi^{(2)}$ and $\chi^{(4)}/\chi^{(2)}$ ratios from the resonance decay compared with no decay of resonances. Note that the mean of the net-strangeness multiplicity is zero due to the imposed strangeness neutrality and isospin asymmetry in the initial state of Au + Au collisions [24]. Therefore, $\chi^{(2)}/\chi^{(1)}$ and $\chi^{(3)}/\chi^{(1)}$ diverges in the case of net-strange multiplicity distributions in the HRG model, which is not shown in Fig. 3.

Figures 4–6 show the energy dependence of the susceptibility ratios for net-baryon, net-charge, and net-strangeness. Figure 4 shows the susceptibility ratios for net baryon without resonance decay, primordial net protons, and net protons from primordial and resonance contributions without weak decays and including weak decay particles in addition to the resonance contributions from strong decay. The resonance

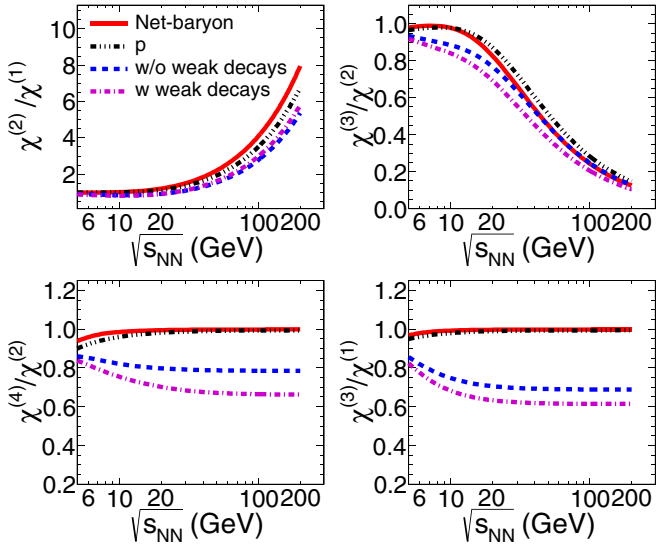

FIG. 4. Variation of susceptibility ratios ($\chi^{(2)}/\chi^{(1)}$, $\chi^{(3)}/\chi^{(2)}$, $\chi^{(4)}/\chi^{(2)}$, and $\chi^{(3)}/\chi^{(1)}$) as a function of $\sqrt{s_{NN}}$ calculated in full phase space for net-baryon without resonance decay, and primordial proton, primordial proton with and without including weak decay in addition to the strongly decaying resonances.

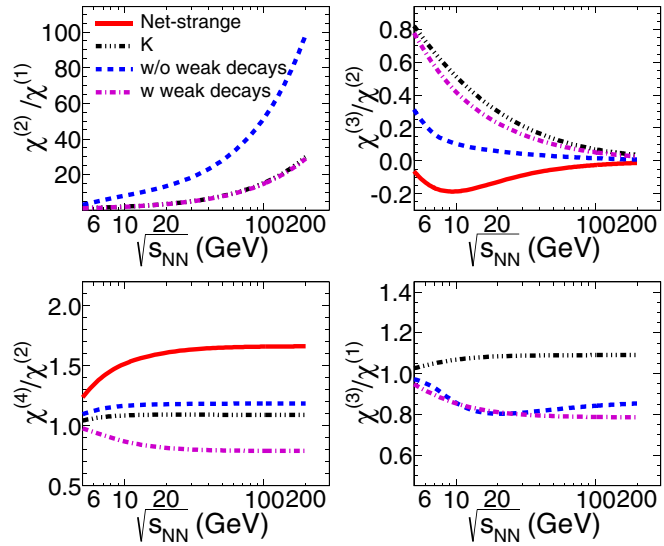

FIG. 6. Variation of susceptibility ratios ($\chi^{(2)}/\chi^{(1)}$, $\chi^{(3)}/\chi^{(2)}$, $\chi^{(4)}/\chi^{(2)}$, and $\chi^{(3)}/\chi^{(1)}$) as a function of $\sqrt{s_{NN}}$ calculated in full phase space for net strange without resonance decay, primordial kaons, and primordial kaons with and without including weak decay in addition to the strongly decaying resonances.

decay contributions are calculated by using full decay contributions as expressed in Eqs. (11)–(13). We consider K^0, $\bar{K}^0$, η^0, Λ^0, $\Sigma^{\pm}$, Σ^0, Ξ^-, Ξ^0, and Ω^- and their antiparticles as weak-decay particles. In Ref. [32], these particles were considered as stable particles and only strongly decaying particles were considered in the resonance decay. In the present work we explicitly considered their weak decays in addition to the strongly decaying particles. There is very little effect

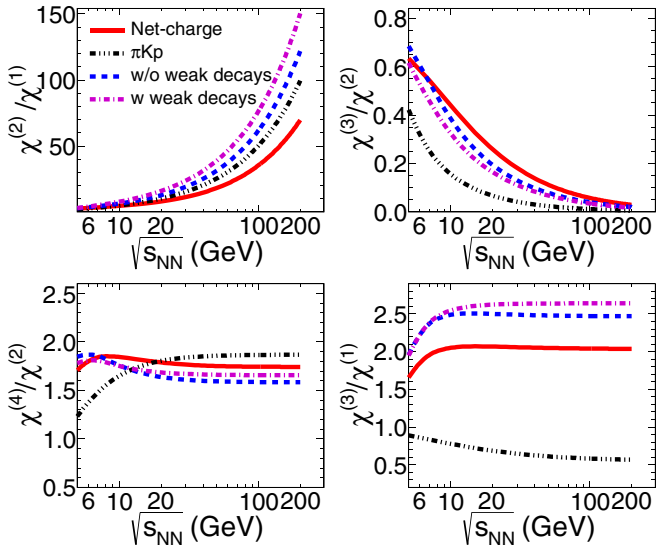

FIG. 5. Variation of susceptibility ratios ($\chi^{(2)}/\chi^{(1)}$, $\chi^{(3)}/\chi^{(2)}$, $\chi^{(4)}/\chi^{(2)}$, and $\chi^{(3)}/\chi^{(1)}$) as a function of $\sqrt{s_{NN}}$ calculated in full phase space for net charge without resonance decay, primordial charged particles (π, K, p), and primordial charged particles with and without including weak decay in addition to the strongly decaying resonances.

on the $\chi^{(2)}/\chi^{(1)}$ ratio for all the energies, but the $\chi^{(3)}/\chi^{(2)}$, $\chi^{(4)}/\chi^{(2)}$, and $\chi^{(3)}/\chi^{(1)}$ ratios further decrease at all $\sqrt{s_{NN}}$ as compared with the values obtained when excluding weak decays. Similarly, Fig. 5 shows the susceptibility ratios for net-charge without decay of resonances, primordial π, K, p, and contributions from strongly decaying resonances both with and without weak decays. There is visible difference between the results with and without inclusion of weak decays. Figure 6 shows the susceptibility ratios for net strangeness without decay of resonances, only primordial kaons, with and without inclusion of weak decays in addition to the contribution from strongly decaying resonances. There is significant difference in the susceptibility ratios with and without inclusion of weak-decay contributions except for the $\chi^{(3)}/\chi^{(1)}$ ratio. For all cases, net-baryon, net-charge, and net-strangeness, it is important to consider weak-decay contributions in addition to the strongly decaying particles while comparing model calculations with the experimental observables. Without decay of resonances and primordial contributions in Figs. 4–6, the results are same as shown in Figs. 1–3.

Figures 7–9 show the variation of susceptibility ratios as a function of $\sqrt{s_{NN}}$ for various p_T acceptances for net-baryon, net-charge, and net-strangeness. The ratios without resonance decay are also shown for comparison. The p_T-acceptance cuts have been applied to the stable particles only and the resonances are taken over the full p_T range. We have also shown another case where the p_T cut is applied to all the particles (stable as well as resonances). Although there is significant difference between the results with and without resonance decay, the p_T acceptance has very minimal effect on the susceptibility ratios after inclusion of resonance decay for all conserved quantities. In Ref. [25], which was studied without taking resonance decay into account, a clear p_T

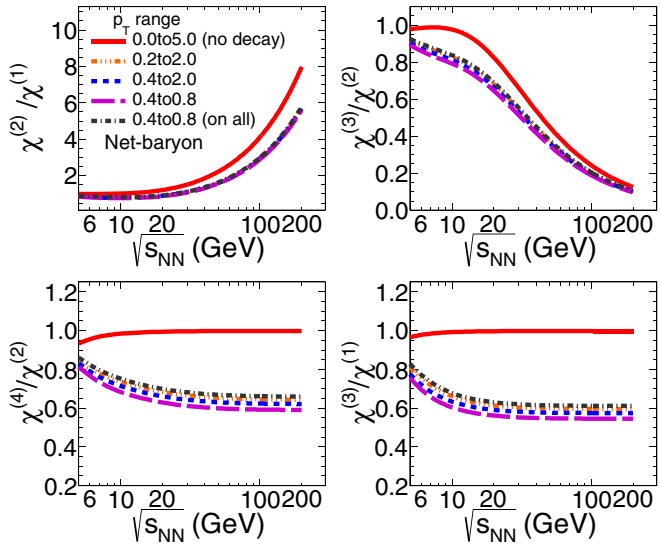

FIG. 7. Collision-energy dependence of susceptibility ratios ($\chi^{(2)}/\chi^{(1)}$, $\chi^{(3)}/\chi^{(2)}$, $\chi^{(4)}/\chi^{(2)}$, and $\chi^{(3)}/\chi^{(1)}$) for net protons for different p_T acceptances within $|\eta| < 0.5$. The results are for primordial protons with resonance decay including weak-decay resonances.

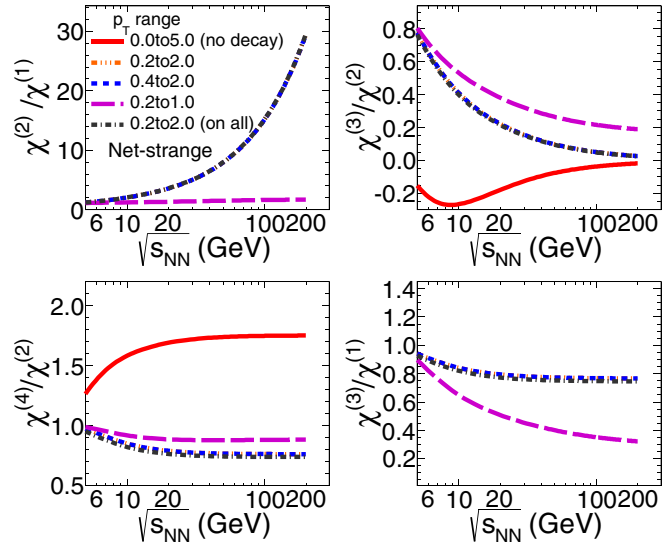

FIG. 9. Collision-energy dependence of susceptibility ratios ($\chi^{(2)}/\chi^{(1)}$, $\chi^{(3)}/\chi^{(2)}$, $\chi^{(4)}/\chi^{(2)}$, and $\chi^{(3)}/\chi^{(1)}$) for net kaons for different p_T acceptances within $|\eta| < 0.5$. The results are for primordial kaons with resonance decay including weak-decay resonances.

dependence was observed for net-charge and net-strangeness cases at all collision energies. In reality, the acceptance cuts should be applied separately on the daughters of resonances. The resonance may be produced in full acceptance which can be outside the experimental acceptance, still the decay daughters have a chance to be accepted within the experimental acceptance because of their decay kinematics. It was mentioned in Ref. [32] that, due to the elastic scatterings in the thermally equilibrated hadronic phase, the kinematic cuts affect the same manner for the primordial particle and antiparticle from the resonance decay. However, this may not be true when the detector will have asymmetric azimuthal acceptance.

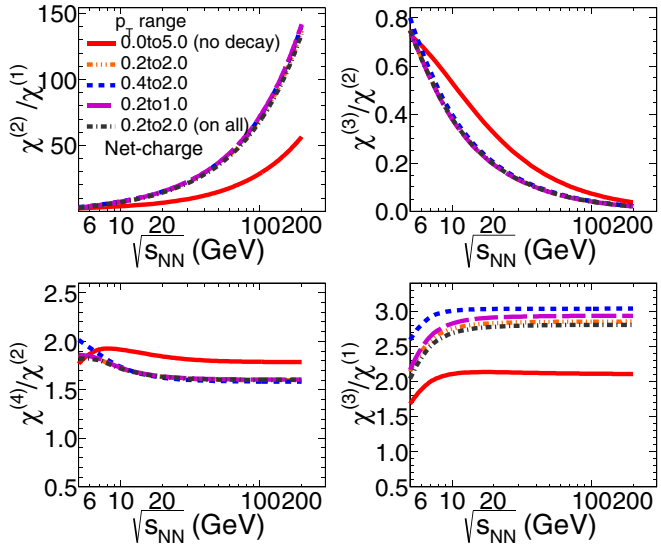

FIG. 8. Collision-energy dependence of susceptibility ratios ($\chi^{(2)}/\chi^{(1)}$, $\chi^{(3)}/\chi^{(2)}$, $\chi^{(4)}/\chi^{(2)}$, and $\chi^{(3)}/\chi^{(1)}$) for net charge for different p_T acceptances with $|\eta| < 0.5$. The results are for primordial charged particles (π, K, p) with resonance decay including weak-decay resonances.

IV. COMPARISON WITH EXPERIMENTAL MEASUREMENTS

Experimentally measured moments (M, σ, S, κ) of the net distributions are related to the susceptibilities as follows: $\sigma^2/M \sim \chi^{(2)}/\chi^{(1)}$, $S\sigma \sim \chi^{(3)}/\chi^{(2)}$, $\kappa\sigma^2 \sim \chi^{(4)}/\chi^{(2)}$. Figure 10 shows the energy dependence of σ^2/M, $S\sigma$, and $\kappa\sigma^2$ of net-proton distribution for central (0%–5%) Au + Au collisions measured by the STAR experiment [17]. The experimental data are studied within midrapidity ($|y| < 0.5$) and p_T range 0.4 to 0.8 GeV/c. The data are compared with the HRG calculations with no decay of resonances, only primordial protons, and resonance decay with and without inclusion of weak-decay contributions in addition to the contribution from strongly decaying resonances within the same experimental acceptance. Note that we have applied the same p_T acceptance cuts to the primordial and to the resonances. The HRG calculations without resonance decay fail to explain σ^2/M at higher collision energies and $S\sigma$ values at lower $\sqrt{s_{NN}}$. The σ^2/M values are well described by considering only primordial protons but overestimate the $S\sigma$ and $\kappa\sigma^2$ values. The ratio σ^2/M calculated in HRG with resonance decay along with inclusion of weak-decay contributions are closer to the experimental values. The $S\sigma$ values lie between resonance decays with and without inclusion of weak decays. The $\kappa\sigma^2$ values at lower $\sqrt{s_{NN}}$ are better described by inclusion of weak decays. For higher collision energy (above 30 GeV), the HRG model under-predicts the experimental values. This may be because of the regeneration of the resonances at higher collision energies, as observed in Refs. [32,35]. Hence

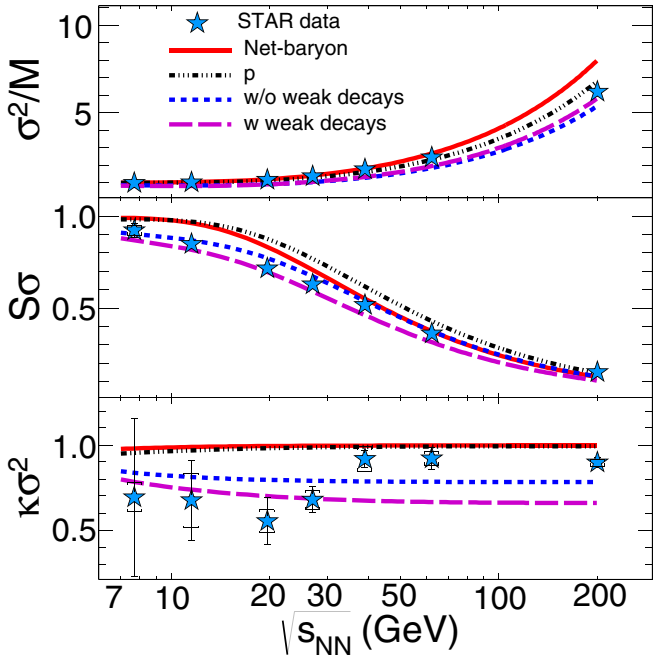

FIG. 10. The collision energy dependence of σ^2/M, $S\sigma$, and $\kappa\sigma^2$ of the net baryon calculated using HRG model including resonance decay contributions. The model calculations are compared with the experimental net proton cumulant ratios for the most-central (0%–5%) Au + Au collisions by the STAR experiment.

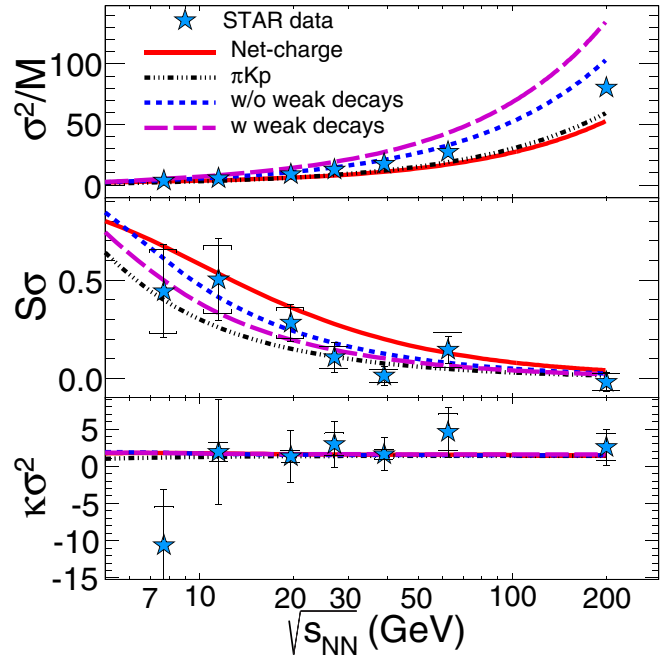

FIG. 11. The collision energy dependence of σ^2/M, $S\sigma$, and $\kappa\sigma^2$ of the net-charge calculated by using HRG model including resonance-decay contributions. The model calculations are compared with the experimental net-charge cumulant ratios for the most-central (0%–5%) Au + Au collisions by the STAR experiment.

it is important to consider the weak decays in addition to the strongly decaying resonances in the HRG model while comparing with experimental data.

Figure 11 shows the energy dependence of σ^2/M, $S\sigma$, and $\kappa\sigma^2$ of net-charge distributions for the most-central (0%–5%) Au + Au collisions within $|\eta| < 0.5$ and a p_T range within 0.2 to 2.0 GeV/c measured by the STAR experiment [16]. The experimental net-charge results are compared with the HRG calculations considering without resonance decay, only charged stable particles (π, K, p), and resonance decay with and without inclusion of weak decays along with strongly decaying resonances. The HRG results for σ^2/M without resonance decay and considering only primordial particles shows lower values compared with the experimental data, whereas the HRG calculations with resonance decay overestimate the experimental data. Inclusion of weak decays further worsen the agreement with the experimental data at higher $\sqrt{s_{NN}}$. The experimental $S\sigma$ and $\kappa\sigma^2$ values are explained by all cases of HRG because of the large uncertainties in the measured experimental data.

Figure 12 shows the collision energy dependence of σ^2/M, $S\sigma$, and $\kappa\sigma^2$ of the net-charge distribution for the most-central bin (0%–5%) in Au + Au collisions measured by PHENIX experiment [15]. The experimental measurements are within $|\eta| < 0.35$ and p_T between 0.3 and 2.0 GeV/c. The experimental data are compared with the HRG calculations considering no decay of resonances, only primordial charged hadrons (π, K, p), with and without inclusion of weak decays in the resonance decay. The kinematic acceptance cuts applied to the HRG calculations are same as in experimental data. As

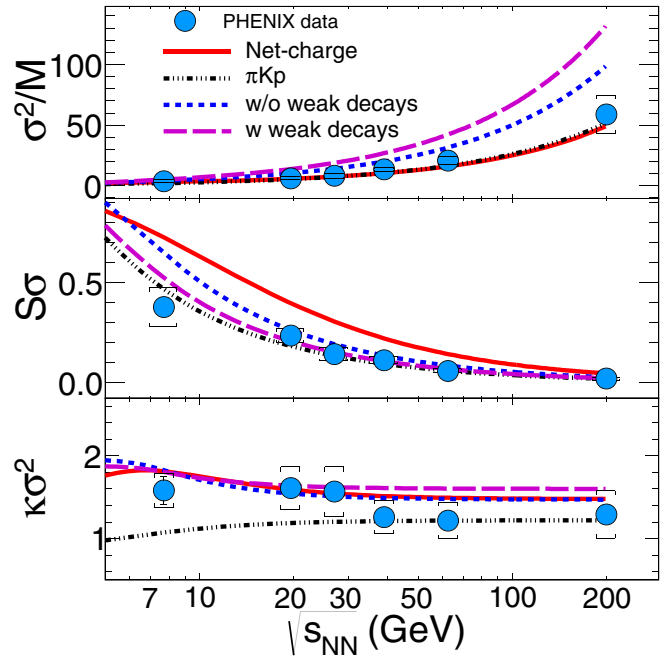

FIG. 12. The collision energy dependence of σ^2/M, $S\sigma$, and $\kappa\sigma^2$ of the net charge calculated by using HRG model including resonance decay contributions. The model calculations are compared with the experimental net-charge cumulant ratios for the most-central (0%–5%) Au + Au collisions by the PHENIX experiment.

observed in STAR net-charge results, the HRG calculations without resonance decay are more close to the experimental σ^2/M values. Inclusion of resonance decay overestimate the experimental data. Inclusion of weak decay in the resonance decay further deviates from the experimental values. The disagreement in σ^2/M between experimental data and the HRG may be because of the acceptance cuts. As mentioned before, we applied the kinematic acceptance cuts on the resonance not on their daughter particles. However, if we consider the resonances in full phase space for a 4π detector then the neutral resonances will not contribute to the net-charge fluctuations. For example, the case ρ^0, K^{*0}, or Λ^0, if we measure the daughter particles in full phase space, they will also not contribute to the net-charge fluctuation. This may be one of the reasons why σ^2/M are not explained by HRG model with resonance decay. The HRG calculations without resonance decay fails to explain the experimental $S\sigma$ at all $\sqrt{s_{NN}}$. The $S\sigma$ are well explained by resonance decay with weak-decay contributions. In this case also, results from only primordial charged particles are more close to the experimental data. The $\kappa\sigma^2$ values are well explained by HRG with resonance decay within the experimental uncertainties at all energies studied. The $\kappa\sigma^2$ values without resonance decay also shows similar results as with resonance decay. However, considering only primordial charged particles explain the experimental data very well at higher $\sqrt{s_{NN}}$ but fails to explain them at lower collision energies.

V. SUMMARY

In conclusion, we studied the effect of resonance decay on conserved number fluctuations by using a hadron resonance gas model. There is a significant effect of resonance decay as compared to no decay of resonances for all the conserved number fluctuations. The effect of considering primordial particles with average decay contributions of the resonances are studied. There is small effect whether we consider average decay or full decay of resonances. The inclusion of weak resonance decays in addition to the strongly decaying particles show visible differences compared to no inclusion of weak decays. The effect of different p_T acceptance cuts on the resonance decay are very minimal for all the conserved numbers. The experimental data for net proton and net charge are compared with the HRG calculations, which are estimated within the similar kinematic acceptance as in the experiment. The cumulant ratios of net-proton distributions are better explained by considering the resonance decay contributions, and the agreement further improves by inclusion of weak resonance decays. The HRG calculations for net charge with resonance decay overestimates the experimental σ^2/M values. However, the $S\sigma$ and $\kappa\sigma^2$ of net-charge experimental values are well explained by HRG calculations with resonance decay, which further improves by including the weak decays. Hence, it is important to consider resonance decays and with weak-decay resonance contribution before comparing the model calculations with experimental data.

[1] M. A. Stephanov, K. Rajagopal, and E. V. Shuryak, Phys. Rev. Lett. **81**, 4816 (1998).
[2] M. G. Alford, K. Rajagopal, and F. Wilczek, Phys. Lett. B **422**, 247 (1998).
[3] M. A. Stephanov, Phys. Rev. Lett. **76**, 4472 (1996).
[4] Y. Aoki, G. Endrodi, Z. Fodor, S. D. Katz, and K. K. Szabo, Nature (London) **443**, 675 (2006).
[5] M. A. Stephanov, Prog. Theor. Phys. Suppl. **153**, 139 (2004); Int. J. Mod. Phys. A **20**, 4387 (2005).
[6] Z. Fodor and S. D. Katz, J. High Energy Phys. 04 (2004) 050.
[7] M. A. Stephanov, K. Rajagopal, and E. V. Shuryak, Phys. Rev. D **60**, 114028 (1999).
[8] V. Koch, A. Majumder, and J. Randrup, Phys. Rev. Lett. **95**, 182301 (2005).
[9] M. Asakawa, U. W. Heinz, and B. Muller, Phys. Rev. Lett. **85**, 2072 (2000).
[10] M. Asakawa, S. Ejiri, and M. Kitazawa, Phys. Rev. Lett. **103**, 262301 (2009).
[11] S. Ejiri, F. Karsch, and K. Redlich, Phys. Lett. B **633**, 275 (2006).
[12] A. Bazavov, H. T. Ding, P. Hegde, O. Kaczmarek, F. Karsch, E. Laermann, S. Mukherjee, P. Petreczky *et al.*, Phys. Rev. Lett. **109**, 192302 (2012).
[13] S. Borsanyi, Z. Fodor, S. D. Katz, S. Krieg, C. Ratti, and K. K. Szabo, Phys. Rev. Lett. **113**, 052301 (2014).
[14] P. Alba, W. Alberico, R. Bellwied, M. Bluhm, V. Mantovani Sarti, M. Nahrgang, and C. Ratti, Phys. Lett. B **738**, 305 (2014).
[15] A. Adare *et al.* (PHENIX Collaboration), Phys. Rev. C **93**, 011901 (2016).
[16] L. Adamczyk *et al.* (STAR Collaboration), Phys. Rev. Lett. **113**, 092301 (2014).
[17] L. Adamczyk *et al.* (STAR Collaboration), Phys. Rev. Lett. **112**, 032302 (2014).
[18] M. M. Aggarwal *et al.* (STAR Collaboration), Phys. Rev. Lett. **105**, 022302 (2010).
[19] B. Berdnikov and K. Rajagopal, Phys. Rev. D **61**, 105017 (2000).
[20] P. Braun-Munzinger, K. Redlich, and J. Stachel, in *Quark Gluon Plasma 3*, edited by R. C. Hwa (World Scientific, Singapore, 2004), p. 491.
[21] J. Cleymans, H. Oeschler, K. Redlich, and S. Wheaton, Phys. Rev. C **73**, 034905 (2006).
[22] A. Andronic, P. Braun-Munzinger, K. Redlich, and J. Stachel, J. Phys. G **38**, 124081 (2011).
[23] V. V. Begun, M. I. Gorenstein, M. Hauer, V. P. Konchakovski, and O. S. Zozulya, Phys. Rev. C **74**, 044903 (2006).
[24] F. Karsch and K. Redlich, Phys. Lett. B **695**, 136 (2011).
[25] P. Garg, D. K. Mishra, P. K. Netrakanti, B. Mohanty, A. K. Mohanty, B. K. Singh, and N. Xu, Phys. Lett. B **726**, 691 (2013).
[26] J. Fu, Phys. Lett. B **722**, 144 (2013).
[27] P. Rau, J. Steinheimer, S. Schramm, and H. Stöcker, Phys. Lett. B **733**, 176 (2014).
[28] P. K. Netrakanti, X. F. Luo, D. K. Mishra, B. Mohanty, A. Mohanty, and N. Xu, Nucl. Phys. A **947**, 248 (2016).
[29] D. K. Mishra, P. Garg, and P. K. Netrakanti, Phys. Rev. C **93**, 024918 (2016).
[30] T. J. Tarnowsky and G. D. Westfall, Phys. Lett. B **724**, 51 (2013).
[31] G. D. Westfall, Phys. Rev. C **92**, 024902 (2015).

[32] M. Nahrgang, M. Bluhm, P. Alba, R. Bellwied, and C. Ratti, Eur. Phys. J. C **75**, 573 (2015).
[33] V. Koch, in *Relativistic Heavy Ion Physics*, edited by R. Stock (Springer, Heidelberg, 2010), pp. 626–652.
[34] S. Jeon and V. Koch, Phys. Rev. Lett. **83**, 5435 (1999).
[35] M. Kitazawa and M. Asakawa, Phys. Rev. C **86**, 024904 (2012); **86**, 069902(E) (2012).